Oxygen Surface Functionalization of Graphene Nanoribbons for Transport Gap Engineering

Alessandro Cresti,[†,*] Alejandro Lopez-Bezanilla,[‡] Pablo Ordejón,[§] and Stephan Roche[⊥,∥]

[†]IMEP-LAHC (UMR CNRS/INPG/UJF 5130), Grenoble INP Minatec, 3 Parvis Louis Néel, BP 257, F-38016 Grenoble, France, [‡]Oak Ridge National Laboratory, One Bethel Valley Road, Oak Ridge, Tennessee 37831-6493, United States, [§]CIN2 (CSIC-ICN) Barcelona, Campus Universitat Autonoma de Barcelona, E-08193 Bellaterra, Spain, [⊥]CIN2 (ICN-CSIC) and Universitat Autonoma de Barcelona, Catalan Institute of Nanotechnology, Campus de la UAB, 08193 Bellaterra (Barcelona), Spain, and [∥]ICREA, Institució Catalana de Recerca i Estudis Avancats, 08010 Barcelona, Spain

ABSTRACT We numerically investigate the impact of epoxide adsorbates on the transport properties of graphene nanoribbons with width varying from a few nanometers to 15 nm. For the wider ribbons, a scaling analysis of conductance properties is performed for adsorbate density ranging from 0.1% to 0.5%. Oxygen atoms introduce a large electron–hole transport asymmetry with mean free paths changing by up to 1 order of magnitude, depending on the hole or electron nature of charge carriers. The opening of a transport gap on the electron side for GNRs as wide as 15 nm could be further exploited to control current flow and achieve larger ON/OFF ratios, despite the initially small intrinsic energy gap. The effect of the adsorbates in narrow ribbons is also investigated by full *ab initio* calculations to explore the limit of ultimate downsized systems. In this case, the inhomogeneous distribution of adsorbates and their interplay with the ribbon edge are found to play an important role.

KEYWORDS: graphene nanoribbons · functionalization · quantum transport · mobility gap · numerical simulation

Graphene nanoribbons (GNRs) are often seen as promising building blocks for engineering graphene-based field effect transistors (GNR-FET) due to their unique electronic properties that can be modified by altering their width and chemical composition.[1] However, the presence of a tunable confinement-induced energy bandgap is also concomitant with a charge mobility reduced by orders of magnitudes, when compared to that of zero-bandgap two-dimensional graphene.[2] Actually, the smaller the width of the ribbon, the larger the effect of edge disorder and the worse the mobility is.[3−6] The quest for fabricating efficient GNR-FETs requires a trade-off between a sufficiently wide energy gap and a reasonably large charge mobility. To circumvent such a hurdle, the use of bilayer graphene has been proposed since interlayer interaction results in an energy bandgap opening, although its value remains too small for achieving an ON/OFF ratio large enough for digital electronics.[7] An alternative could be the use of chemical doping (beyond chemical sensing applications)[8] by substituting carbon atoms with doping impurities. Biel and co-workers[9,10] demonstrated that boron- and nitrogen-doped GNRs show large mobility gaps and a strong electron–hole transport asymmetry, which can be further tuned by changing the impurity density and the ribbon length, while keeping a wide ribbon of several tens of nanometers. This would enable the massive integration of individual devices and the design of circuits by using the state-of-the-art lithography techniques. However, the realization of chemical substitutions of carbon atoms in GNRs is a challenging issue, and, to date, little progress has been made, with almost no control of the dopant density.[11−14]

In this work, we show that surface functionalization, easier to achieve experimentally, can yield large electron–hole conduction asymmetry and transport gaps, thus bringing new building blocks to the all-carbon nanoelectronics. We focus on epoxide adsorbates, easily produced by ozone decomposition on graphene surface.[15,16] By using tight-binding parameters extracted from first-principles calculations on two-dimensional graphene, transport simulations on disordered ribbons with widths ranging from 5 to 15 nm are achieved. Our findings suggest that functionalization with oxygen atoms in the epoxide configuration of the GNRs of widths on the order of a few tens of nanometers could improve the usefulness of devices by means of electronic current ON/OFF switch based on a transport gap.

We explain the conduction asymmetry in terms of the oxygen–graphene bond details, which are implicitly described by the multiorbital tight-binding model. Farmer and co-workers[17] showed that electron–hole

* Address correspondence to crestial@minatec.inpg.fr.

Received for review September 16, 2011 and accepted October 10, 2011.

Published online October 10, 2011
10.1021/nn203573y

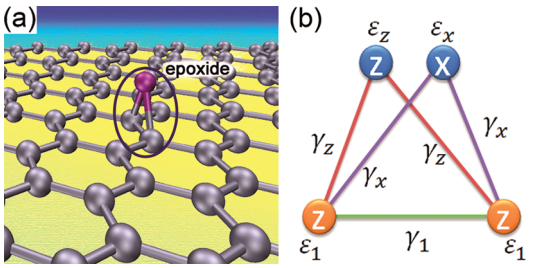

Figure 1. (a) Epoxide oxygen adsorbed on the surface of a graphene nanoribbon. (b) Adopted tight-binding model.

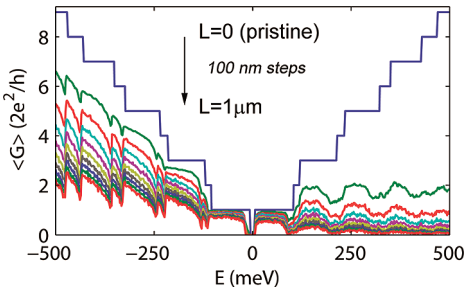

Figure 2. Average conductance of a 125-aGNR in the presence of epoxide groups with density n = 0.1% and for length L of the disordered region up to 1 μm in steps of 100 nm. The average is performed over 50 random configurations.

conduction asymmetry can arise from the misalignment of electrodes and channel charge neutrality points, which results in imbalanced electron injection. With respect to this model, the asymmetry that we predict is stronger and related to the rehybridization of the atomic orbitals of the carbon atoms to which the functional groups are attached, and to the asymmetric distribution of the charge shared between oxygen and carbon atoms. We also investigate the case of ultranarrow ribbons, whose high-quality fabrication has recently been achieved by pioneering chemical techniques.[18−23] To this aim, we make use of transport simulations based on accurate full *ab initio* Hamiltonians as obtained from the SIESTA code.[24,25] The results evidence the strong role of the inhomogeneous distribution of adsorbates and the increasing variability effects in the ultimate downsized limit.

RESULTS AND DISCUSSION

Tight-Binding Model for Epoxide Oxygen on the Graphene Surface. The system under study is a functionalized graphene nanoribbon of length L and width W connected to source and drain contacts by two perfect leads made up of pristine nanoribbons of the same width. The density of adsorbates on the ribbon surface over the total number of carbon atoms is indicated by n. We describe pristine graphene nanoribbons by a standard first-neighbor tight-binging Hamiltonian with a single p_z orbital per atom, zero on-site energy, and hopping $\gamma_0 = -2.6$ eV

$$H = \sum_{\langle ij \rangle} \gamma_0 c_i^+ c_i \qquad (1)$$

where $\langle ij \rangle$ indicates couples of neighbor atoms, while c_i^+ and c_i represent the creation and annihilation operators for electrons in the p_z orbital of the atom i. At the edges of armchair ribbons, γ_0 is increased by 12% to take into account the shrinkage of the carbon−carbon bonds.[26]

To include the presence of epoxide adsorbates on the system surface (see Figure 1a), we adopt the model developed in ref 16, where the tight-binding parameters are obtained from *ab initio* simulations in two-dimensional graphene. As far as wide nanoribbons are considered ($W \geq 5$ nm), the very short-range nature of this disorder allows us to use this model without further adjustment. The case of ultranarrow ribbons requires, however, a substantial refinement of the model, as discussed later on. According to ref 16, the tight-binding model for epoxide oxygen includes the two p_x and p_z oxygen orbitals, which are coupled to the p_z orbitals of its two neighboring carbon atoms. For an oxygen atom over two carbon atoms p and q, the Hamiltonian is

$$\begin{aligned} H_{pq}^{\text{epoxide}} &= \varepsilon_1(c_p^+ c_p + c_q^+ c_q) + \varepsilon_x d_x^+ d_x + \varepsilon_z d_z^+ d_z \\ &+ \gamma_x(c_p^+ d_x + d_x^+ c_p + c_q^+ d_x + d_x^+ c_q) + \gamma_x(c_p^+ d_z \\ &+ d_z^+ c_p + c_q^+ d_z + d_z^+ c_q) + \gamma_1(c_p^+ c_q + c_q^+ c_p) \qquad (2) \end{aligned}$$

where d_x and d_y are the field operators for the extra orbitals, $\varepsilon_1 = 1.5$ eV, $\varepsilon_x = -2.5$ eV, $\varepsilon_z = -1$ eV, $\gamma_x = -4.68$ eV, $\gamma_z = 3.9$ eV, and $\gamma_1 = 0$, the latter meaning that the direct coupling between the involved carbon atoms is vanishing (see Figure 1b). These tight-binding parameters were obtained in ref 16 by fitting the *ab initio* band structure of a graphene supercell containing a single epoxide and by testing their validity for larger supercells.

Chemically Induced Electron−Hole Transport Asymmetry in Wide Graphene Nanoribbons. We start to characterize the mesoscopic transport properties of long functionalized nanoribbons by first considering wide GNRs with widths W = 5 nm (41-aGNR), W = 10 nm (83-aGNR), and W = 15 nm (125-aGNR), where 41, 83, and 125 indicate the number of dimer carbon lines that compose the ribbons. We perform a statistical analysis over 50 random configurations for functionalized sections with length L up to 1 μm, by computing the transmission coefficients for disordered ribbons and averaging the results. As an example, Figure 2 reports the average conductance $\langle G \rangle$ as a function of the electron energy E for the W = 15 aGNR in the presence of n = 0.1% of epoxide adsorbates for different lengths L of the disordered ribbon. When L = 0 the ribbon is pristine and, as expected, the conductance is quantized in multiples of $2e^2/h$. As L increases, in steps of 100 nm, the conductance is progressively degraded. The pace of such a degradation is much faster for electrons ($E > 0$)

than for holes ($E < 0$), thus determining a marked asymmetry in the hole and electron regions of the spectrum, as expected from recent literature.[27] In particular, transport turns out to be significantly suppressed at positive energies, with a resulting transport gap. The possibility of tuning this transport gap by varying the degree of functionalization and the width of the ribbons is the main motivation of this study.

In what follows, we analyze systematically this asymmetry and its scaling properties by estimating the mean free path l_e of GNRs as a function of the electron energy for different adsorbate densities and ribbon widths. The mainframe of Figure 3a shows l_e as a function of E for armchair graphene nanoribbons in the presence of $n = 0.1\%$ of adsorbates and for different ribbon widths W. To compare energy regions with the same number of conductive channels, whose onset is indicated by vertical lines in the figure, l_e is plotted as a function of $E \times (10\ \text{nm}/W)$. In other words, the energies for the narrowest and the widest ribbons are rescaled. The energy window around the charge neutrality point (CNP), where l_e is zero, corresponds to the bandgap region of the pristine ribbon. For the same number of active conductive modes, the mean free path increases with W. The likely origin of this upscaling of l_e has to be found in the preservation of the graphene sublattice symmetry, which applies to the case of epoxide defects bonded to two neighboring carbon atoms, and is similar to the analytical results for long-range disorder in metallic carbon nanotubes.[28] The electron mean free path for the 125-aGNR is about 1.5 times that of the 83-aGNR, thus evidencing a linear scaling with W. In the hole region (slightly shifted from CNP), the mean free paths are much closer, in all probability due to the fact that l_e is much larger than the ribbon width itself. The case of the 41-aGNR is more irregular, indicating increased effects of quasi-bound states and correlation phenomena related to the narrow width $W = 5$ nm. The inset of Figure 3a shows l_e for the 10 nm wide nanoribbon (83-aGNR) with increasing adsorbate density (from $n = 0.1\%$ to $n = 0.5\%$). The mean free path roughly scales as $l_e \sim n^{-1}$ for low $n \leq 0.3\%$. The decay is slightly faster in the hole region, thus suggesting the rise of correlation effects and bound states. At higher densities this effect is observed in the whole energy spectrum.

Figure 3b shows l_e for an 84-aGNR with an adsorbate density $n = 0.1\%$, when taking into account some additional thermal averaging at room temperature. Note that the 84-aGNR has a larger bandgap with respect to the 83-aGNR of Figure 3a. This reflects the existence of three families of armchair ribbons constituted of $3m$, $3m+1$, and $3m+2$ dimer lines (where m is an integer), with a different hierarchy of gap and band sequence. The blue line confirms that the impact of epoxide is markedly asymmetric, with much longer l_e in the hole region. To better understand the origin of this behavior and motivated by the topological

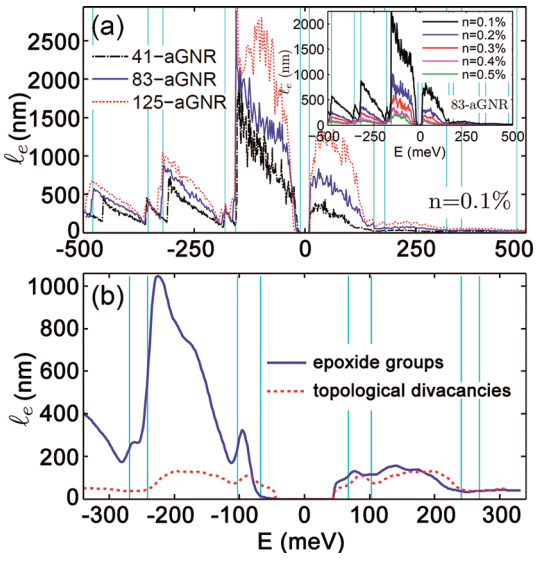

Figure 3. (a) Main frame: Mean free path in the presence of $n = 0.1\%$ of epoxide adsorbates for armchair ribbons of width $W = 5$ nm (41-aGNR), $W = 10$ nm (83-aGNR), and $W = 15$ nm (125-aGNR). The electron energy E is scaled by 10 nm/W. The vertical lines indicate the activation of conductive channels. Inset: Mean free path in the presence of $n = 0.1-0.5\%$ of epoxide adsorbates for an armchair ribbon of width $W \approx 10$ nm (83-aGNR). (b) Mean free path at 300 K in an 84-aGNR in the presence of topological divacancies or epoxide groups with density $n = 0.1\%$.

correspondence of epoxides and divacancies, we also evaluated l_e for these types of defect. The Hamiltonian is obtained by simply removing the p_z orbitals of the carbon atoms corresponding to the divacancies, which we call *topological divacancies* to distinguish them from real divacancies, whose structure is more complex. Since no odd-numbered rings are produced in the structure, the impact on the transport properties is perfectly symmetric in the electron and hole regions; see the red dotted line. The comparison shows that the similarity to the topological divacancies is observed only in the electron region, while the behavior is completely different for $E < 0$.

A closer analysis of the epoxide-adopted tight-binding model helps us clarify the origin of these similarities and differences. By means of the Dyson equation within Green's function formalism, it can be shown that the Hamiltonian (eq 2) is equivalent to the energy-dependent renormalized Hamiltonian

$$\tilde{H}_{pq}^{\text{epoxide}}(E) = \varepsilon(E)(c_p{}^{+}c_p + c_q{}^{+}c_q) + \gamma(E)(c_p{}^{+}c_q + c_q{}^{+}c_p) \quad (3)$$

where

$$\varepsilon(E) = \varepsilon_1 + \frac{\gamma_x{}^2}{E - \varepsilon_x} + \frac{\gamma_z{}^2}{E - \varepsilon_z};$$

$$\gamma(E) = \gamma_1 + \frac{\gamma_x{}^2}{E - \varepsilon_x} + \frac{\gamma_z{}^2}{E - \varepsilon_z} \quad (4)$$

This Hamiltonian explicitly involves only the orbitals of the carbon atoms. The effect of the presence of the

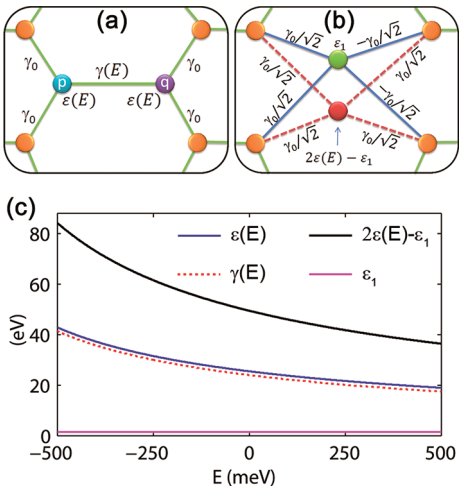

Figure 4. (a) Scheme of the renormalized Hamiltonian. The effect of the two oxygen orbitals on the *p* and *q* carbon atoms is included in the energy-dependent effective on-site ε and hopping γ parameters. (b) Further elaboration of the Hamiltonian obtained by considering the symmetric and antisymmetric combination of the two carbon orbitals. (c) Value of the relevant renormalized on-site and hopping parameters as a function of the energy *E*.

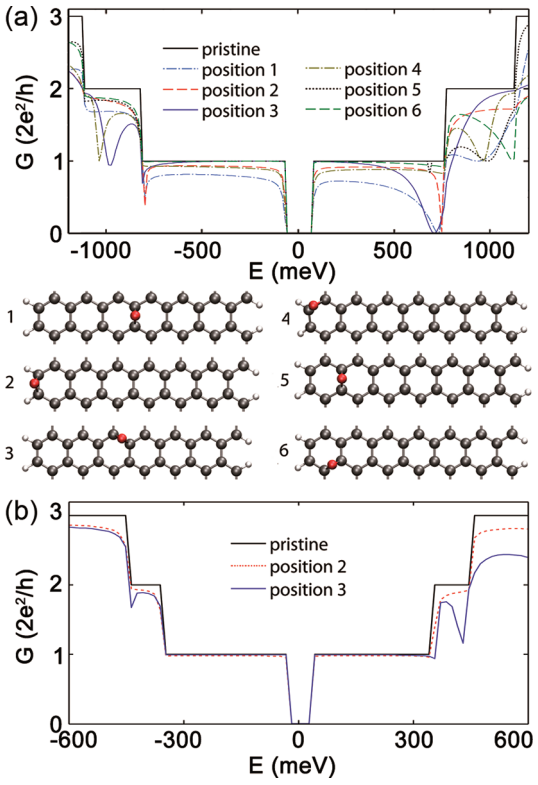

Figure 5. (a) Conductance profiles for a 14-aGNR as a function of the energy of charge carriers for a single epoxide defect at the different positions as indicated. (b) Conductance profiles for a 35-aGRN with an oxygen atom in epoxide configuration for two representative atom positions: the blue line corresponds to the oxygen atom sitting on the ribbon edge (position 2), and the red line to an oxygen atom in the center of the ribbon (position 3).

oxygen orbitals is taken into account by the energy-dependent parameters ε and γ. The scheme of the renormalized system is reported in Figure 4a. With the adopted tight-binding parameters, $\varepsilon(E)$ regularly decreases from about 40 eV at $E = -500$ meV down to about 20 eV at $E = 500$ meV, as shown in Figure 4c. This might suggest that epoxide should behave as a topological divacancy on the hole side and at low energies, because of the high renormalized on-site energies on the two carbon atoms where the adsorbate is placed. However this is not the case, as apparent from Figure 3b. The reason is that also the renormalized coupling between the two carbon atoms $\gamma(E)$ is high and comparable to $\varepsilon(E)$; in fact they only differ by $\varepsilon_1 - \gamma_1 = 1.5$ eV. Therefore the effective on-site energy is not significantly larger than the hopping energy, and no topological vacancy effect is expected.

A further elaboration is necessary to shed light on this issue. By performing a symmetric and an antisymmetric combination of the two orbitals of the involved carbon atoms, the system turns out to be equivalent to that of Figure 4b. The resulting states are now uncoupled from each other, and they are coupled to the p_z orbitals of the four neighbor atoms by $\gamma_0/\sqrt{2}$. The on-site energies are ε_1 for the antisymmetric orbital combination and $2\varepsilon(E) - \varepsilon_1$ for the symmetric one. The corresponding values are shown in Figure 4c. Since this time the hopping energy is much smaller than $2\varepsilon(E) - \varepsilon_1$, we can disregard the symmetric combination and consider it as a topological vacancy. This is indicated by dashed lines in Figure 4b. In contrast, the on-site energy of the antisymmetric combination is constant and equal to ε_1, *i.e.*, comparable to the coupling parameter. As a result, the adsorbate turns out to be roughly equivalent to a couple of pentagonal rings with a common vertex, where the vertex corresponds to the antisymmetric orbital combination. The coupling between the neighbor carbon atoms and the vertex is $\gamma_0/\sqrt{2}$, and the vertex on-site energy is ε_1. Such an equivalent configuration explains the strong electron–hole asymmetry observed for epoxide defects in Figure 3 and the topological divacancy-like behavior at positive energy, when E approaches ε_1.

Functionalized Ultranarrow Graphene Ribbons. To contrast the tight-binding results and examine the borderline case of ultranarrow ribbons, we also perform transport calculations based on full *ab initio* Hamiltonians.[24] The goal is to understand whether the electron–hole asymmetry observed for wide ribbons is robust when reducing the ribbon width below the current lithographic limit. It is also important to understand to what extent different adsorbate distributions within the ribbon entail transport feature modulations. This issue might be crucial at very low concentration of adsorbates and introduce large sample-to-sample differences, with consequent variability effects.

Figure 5a shows the conductance of a 14-aGNR in the presence of a single epoxide at different positions

across the nanoribbon width. As expected, the result is very position dependent, thus highlighting the important interplay between adsorbate and edges. In the region of the first conductance plateau around the charge neutrality point, a slight electron–hole asymmetry develops when the oxygen is close to the center of the ribbon (positions 1 and 3), with a dip around $E = 0.7$ eV. As the epoxide becomes closer to the edges (positions 2, 4, 5, and 6), the antiresonance disappears and the electron–hole symmetry within the first conductive channel is restored. This indicates that, as far as concerns the electron–hole asymmetry effect, bulk disorder is more relevant. However, adsorbates that are very close to the edges (positions 2 and 4) lower the transmission considerably, with possible detrimental effects on the global mobility of ultranarrow ribbons. When two conductive channels are active, *i.e.*, in the energy range where the conductance of the pristine ribbon is on the second plateau, the adsorbate position dependence of the transmission appears more cumbersome. Nevertheless, it is observed that an electron–hole asymmetry is still present, with an overall lower conductance at positive energies.

The computed adsorption energies show that edge functionalization is more favored than the bulk functionalization. For example, the energy difference between configurations 1 and 2 in Figure 5a is 1.11 and 0.44 eV between configurations 1 and 4. This result entails an inhomogeneous distribution of epoxide defects and thus a reduced charge carrier scattering efficiency for ultranarrow ribbons. A Mulliken population analysis reveals that oxygen atoms act as acceptor functional groups with an effective charge transfer of ~0.13 electron.

As the ribbon width increases, the impact of a single impurity in the channel becomes less significant. Figure 5b shows the transmission coefficients for an oxygen atom in epoxide configuration as sitting on the center of a 35-aGNR and on the edge. For the former, the transmission is barely modified with respect to the pristine ribbon on the first electron plateau, whereas a decrease is observed as approaching the transition from the first to the second plateau on the hole side. For an atom sitting on the ribbon edge, a homogeneous and symmetric decreasing of the transmission coefficients is observed. We now briefly consider the case of epoxide-functionalized ultranarrow ribbons with mesoscopic length. Figure 6 reports some transport simulation results from *ab initio* Hamiltonians for 14-aGNRs. To obtain the Hamiltonian of long disordered ribbons, we first perform first-principles calculations of short GNR sections with a single adsorbate at different positions. Then we combine these sections in a random distribution, along with sections of pristine ribbon.[29] By means of real-space renormalization techniques, we are able to evaluate the transport properties of GNRs with lengths up to $L = 1.7\ \mu$m.

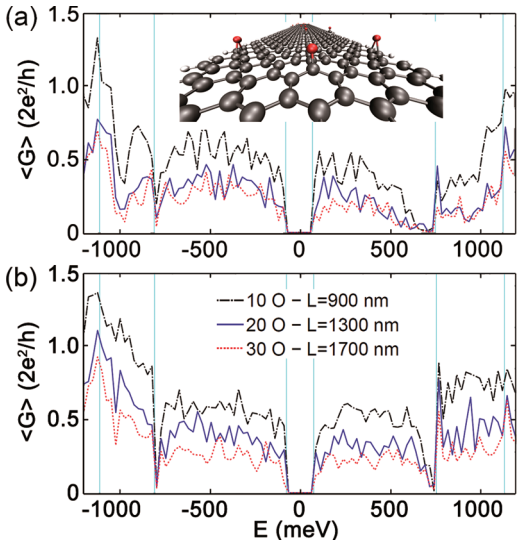

Figure 6. Average conductance (over 20 random configurations) of 14-aGNR in the presence of bulk (a) and edge (b) epoxide functionalization. Different numbers of oxygen atoms and ribbon length are considered.

To better understand the role of edges and narrow ribbons with respect to the case of wide ribbons, we consider two cases where adsorbates are distributed throughout the ribbons (see Figure 6a) or only at edges (see Figure 6b). The first case confirms the electron–hole asymmetry observed for wider ribbons with the tight-binding description. However, at the low adsorbate densities considered, the asymmetry is less marked than for wider GNRs. This fact puts in evidence that, for ultranarrow ribbons, the tight-binding model obtained from *ab initio* simulations of functionalized two-dimensional graphene provides only a qualitative trend of the ribbon transport properties, while the full *ab initio* model is mandatory to obtain quantitative results.

In contrast, the case of adsorbates only along the edges, Figure 6b, shows rather symmetric transport properties in the region of the first conductive channel around the CNP. This is in agreement with the results for a single adsorbate of Figure 5 and indicates that for ultranarrow graphene nanoribbons the opening of an asymmetric transport gap might be compromised due to the higher probability for oxygen atoms to be found at edges rather than in the bulk. The ribbon width where a symmetric-to-asymmetric transmission crossover is expected to occur depends on the oxygen spatial distribution in the bulk and edge regions. The estimation of such a width is beyond the scope of this study since it would require one to perform *ab initio* calculations on wider (above 4–10 nm) ribbons. Finally, the presence of large fluctuations in the curves of Figure 6 shows that, at low density, ultranarrow functionalized ribbons are extremely sensitive to the adsorbate positions, thus entailing possible important variability effects, not suitable for nanoelectronics devices.

CONCLUSION

In conclusion, we have performed a scaling analysis of the electronic transport properties of epoxide-functionalized graphene nanoribbons. For wide ribbons, epoxide functionalization results in strongly asymmetric conductance profiles, with the development of a transport gap in the electron region of the spectrum. The extracted mean free paths are shown to downscale linearly with adsorbate density and to increase with the ribbon width. The marked electron–hole asymmetry, as well as the scaling trend, opens the door for the engineering of charge mobility and mobility gaps, with interesting perspectives in the development of graphene-based nanoelectronics for logic circuits. In the case of ultranarrow ribbons (below 2 nm), our *ab initio*-based findings confirm the asymmetric trend of the conductance when adsorbates are placed all over the ribbon. On the contrary, when they are distributed only along the edges, no asymmetry is observed. Since oxygen atoms tend to arrange themselves along the edges, we conclude that the marked electron–hole transport asymmetry might be significantly weakened for ultranarrow ribbons. Another inconvenience of downsized functionalized ribbons is the strong sample-to-sample fluctuations due to the edges–adsorbate interplay, which might represent an important source of variability for nanoelectronics devices.

METHODS

We obtain the accurate *ab initio* Hamiltonian for ultranarrow ribbons by using a localized atomic-like basis set in the local density approximation (SIESTA code)[24,25] with a double-ζ basis for each atom. The geometry of the different configurations is achieved by relaxing the whole structure until residual forces are smaller than 0.02 eV/Å.

To evaluate the conductance of the system, G, we adopt the standard Green's function formalism, which, at quasi-equilibrium conditions, is

$$G = \frac{2e^2}{h} \times T \text{ with } T = \mathrm{Tr}(\Gamma^{(\mathrm{left})} G^{\mathrm{R}} \Gamma^{(\mathrm{right})} G^{\mathrm{A}}) \qquad (5)$$

where T is the transmission coefficient, $G^{\mathrm{R,A}}$ are the retarded and advanced Green functions projected on the functionalized region, and $\Gamma^{(\mathrm{left/right})}$ are the rate operators corresponding to the left and right contacts. We make use of this approach for both tight-binding and *ab initio* Hamiltonians, as discussed in refs 29 and 30.

The extraction of the mean free path l_e is performed by evaluating the transmission coefficient $T(E,L)$ as a function of the energy E for different lengths L of the functionalized section and over a large number of random configurations. According to the statistical criteria reported in refs 31–33, we can identify whether the transport regime is diffusive or localized for a given couple (E,L). In particular, the diffusive transport regime is distinguished by $\langle \Delta T(E) \rangle < \langle T(E) \rangle$, where $\langle T(E) \rangle$ is the average transmission coefficient and $\langle \Delta T(E) \rangle$ is the corresponding standard deviation. This criterion means that the statistical distribution of the transport coefficients corresponding to different disorder configurations is well-defined, with small deviations around its average value. In this regime, the mean free path is obtained from

$$\langle T(E) \rangle = \frac{M}{1 + L/l_e(E)} \Rightarrow l_e(E) = \frac{\langle T(E) \rangle L}{M - \langle T(E) \rangle} \qquad (6)$$

where M is the number of active conductive channels in the contacts, and it is roughly proportional to W. When increasing the length of the disordered region beyond a certain value, the system enters the localized transport regime, which is identified by $\langle \Delta \log T(E) \rangle < \langle \log T(E) \rangle$. In this case, the well-defined statistical distribution is given by the logarithm of the transmission coefficients.

Acknowledgment. The work has been performed under the HPC-EUROPA2 project (project no. 228398) with the support of the European Commission–Capacities Area–Research Infrastructures. This research used resources of the National Center for Computational Sciences at Oak Ridge National Laboratory, which is supported by the Office of Science of the U.S. Department of Energy under Contract No. DE-AC0500OR22750. We are also grateful for the support from the Center for Nanophase Materials Sciences (CNMS), sponsored at Oak Ridge National Laboratory by the Division of Scientific User Facilities, U.S. S.R. acknowledges the NANOSIM-GRAPHENE Project No. ANR-09-NANO-016-01. A.C. acknowledges the support of Fondation Nanosciences *via* the RTRA Dispograph project. P.O. acknowledges support from Spanish MICINN Grant No. FIS2009-12721-C04-01.

REFERENCES AND NOTES

1. Schwierz, F. Graphene Transistors. *Nat. Nanotechnol.* **2010**, *5*, 487–496.
2. Geim, A. K.; Novoselov, K. S. The Rise of Graphene. *Nat. Mater.* **2007**, *6*, 183–191.
3. Li, X.; Wang, X.; Zhang, L.; Lee, S.; Dai, H. Chemically Derived, Ultrasmooth Graphene Nanoribbon Semiconductors. *Science* **2008**, *319*, 1229–1232.
4. Wang, X.; Ouyang, Y.; Li, X.; Wang, H.; Guo, J.; Dai, H. Room-Temperature All-Semiconducting Sub-10-nm Graphene Nanoribbon Field-Effect Transistors. *Phys. Rev. Lett.* **2008**, *100*, 206803.
5. Cresti, A.; Nemec, N.; Biel, B.; Niebler, G.; Triozon, F.; Cuniberti, G.; Roche, S. Charge Transport in Disordered Graphene-Based Low Dimensional Materials. *Nano Res.* **2008**, *1*, 361–394.
6. Roche, S. Nanoelectronics: Graphene Gets a Better Gap. *Nat. Nanotechnol.* **2011**, *6*, 8–9.
7. Szafranek, B. N.; Schall, D.; Otto, M.; Neumaier, D.; Kurz, H. High On/Off Ratios in Bilayer Graphene Field Effect Transistors Realized by Surface Dopants. *Nano Lett.* **2011**, *11*, 2640–2643.
8. Wehling, T. O.; Novoselov, K. S.; Morozov, S. V.; Vdovin, E. E.; Katsnelson, M. I.; Geim, A. K.; Lichtenstein, A. I. Molecular Doping of Graphene. *Nano Lett.* **2008**, *8*, 173–177.
9. Biel, B.; Triozon, F.; Blase, X.; Roche, S. Chemically Induced Mobility Gaps in Graphene Nanoribbons: A Route for Upscaling Device Performances. *Nano Lett.* **2009**, *9*, 2725–2729.
10. Roche, S.; Biel, B.; Cresti, A.; Triozon, F. Chemically Enriched Graphene-Based Switching Devices: A Novel Principle Driven by Impurity-Induced Quasibound States and Quantum Coherence. *Physica E (Amsterdam, Neth.)*, in press doi: 10.1016/j.physe.2011.06.008.
11. Ahlgren, E. H.; Kotakoski, J.; Krasheninnikov, A. V. Atomistic Simulations of the Implantation of Low-Energy Boron and Nitrogen Ions into Graphene. *Phys. Rev. B* **2011**, *83*, 115424.
12. Guo, B.; Liu, Q.; Chen, E.; Zhu, H.; Fang, L.; Gong, J. R. Controllable N-Doping of Graphene. *Nano Lett.* **2010**, *10*, 4975–4980.

13. Deng, D.; Pan, X.; Yu, L.; Cui, Y.; Jiang, Y.; Qi, J.; Li, W.-X.; Fu, Q.; Ma, X.; Xue, O.; *et al*. Towards N-Doped Graphene *via* Solvothermal Synthesis. *Chem. Mater.* **2011**, *23*, 1188–1193.
14. Li, X.; Wang, H.; Robinson, J. T.; Sanchez, H.; Diankov, G.; Dai, H. Simultaneous Nitrogen Doping and Reduction of Graphene Oxide. *J. Am. Chem. Soc.* **2009**, *131*, 15939–15944.
15. Moser, J.; Tao, H.; Roche, S.; Alzina, F.; Sotomayor Torres, C. M.; Bachtold, A. Magnetotransport in Disordered Graphene Exposed to Ozone: From Weak to Strong Localization. *Phys. Rev. B* **2010**, *81*, 205445.
16. Leconte, N.; Moser, J.; Ordejón, P.; Tao, H.; Lherbier, A.; Bachtold, A.; Alsina, F.; Sotomayor Torres, C. M.; Charlier, J.-C.; Roche, S. Damaging Graphene with Ozone Treatment: A Chemically Tunable Metal-Insulator Transition. *ACS Nano* **2010**, *4*, 4033–4038.
17. Farmer, D. B.; Golizadeh-Mojarad, R.; Perebeinos, V.; Lin, Y.-M.; Tulevsky, G. S.; Tsang, J. C.; Avouris, P. Chemical Doping and Electron-Hole Conduction Asymmetry in Graphene Devices. *Nano Lett.* **2009**, *9*, 388–392.
18. Xie, L.; Wang, H.; Jin, C.; Wang, X.; Jiao, L.; Suenaga, K.; Dai, H. Graphene Nanoribbons from Unzipped Carbon Nanotubes: Atomic Structures, Raman Spectroscopy, and Electrical Properties. *J. Am. Chem. Soc.* **2011**, *133*, 10394–10397.
19. Xie, L.; Jiao, L.; Dai, H. Selective Etching of Graphene Edges by Hydrogen Plasma. *J. Am. Chem. Soc.* **2010**, *132*, 14751–14753.
20. Jiao, L.; Zhang, L.; Ding, L.; Liu, J.; Dai, H. Aligned Graphene Nanoribbons and Crossbars from Unzipped Carbon Nanotubes. *Nano Res.* **2010**, *3*, 387–394.
21. Jiao, L.; Wang, X.; Diankov, G.; Wang, H.; Dai, H. Facile Synthesis of High-Quality Graphene Nanoribbons. *Nat. Nanotechnol.* **2010**, *5*, 321–325.
22. Kosynkin, D. V.; Higginbotham, A. L.; Sinitskii, A.; Lomeda, J. R.; Dimiev, A.; Price, B. K.; Tour, J. M. Longitudinal Unzipping of Carbon Nanotubes to Form Graphene Nanoribbons. *Nature* **2009**, *458*, 872–876.
23. Shinde, D. B.; Debgupta, J.; Kushwaha, A.; Aslam, M.; Pillai, V. K. Electrochemical Unzipping of Multi-Walled Carbon Nanotubes for Facile Synthesis of High-Quality Graphene Nanoribbons. *J. Am. Chem. Soc.* **2011**, *133*, 4168–4171.
24. Ordejón, P.; Artacho, E.; Soler, J. M. Self-Consistent Order-N Density-Functional Calculations for Very Large Systems. *Phys. Rev. B* **1996**, *53*, R10441–R10444.
25. Soler, J. M.; Artacho, E.; Gale, J. D.; García, A.; Junquera, J.; Ordejón, P.; Sánchez-Portal, D. The SIESTA Method for *Ab Initio* Order-N Materials Simulation. *J. Phys.: Condens. Matter* **2002**, *14*, 2745.
26. Son, Y. W.; Cohen, M. L.; Louie, S. G. Energy Gaps in Graphene Nanoribbons. *Phys. Rev. Lett.* **2006**, *97*, 216803.
27. Ihnatsenka, S.; Kirczenow, G. Dirac Point Resonances Due to Atoms and Molecules Adsorbed on Graphene and Transport Gaps and Conductance Quantization in Graphene Nanoribbons with Covalently Bonded Adsorbates. *Phys. Rev. B* **2011**, *83*, 245442.
28. White, C. T.; Todorov, T. N. T. Carbon Nanotubes as Long Ballistic Conductors. *Nature* **1998**, *393*, 240–242.
29. Lopez-Bezanilla, A.; Triozon, F.; Roche, S. Chemical Functionalization Effects on Armchair Graphene Nanoribbon Transport. *Nano Lett.* **2009**, *9*, 2537–2541.
30. Triozon, F.; Lambin, Ph.; Roche, S. Electronic Transport Properties of Carbon Nanotube Based Metal/Semiconductor/Metal Intramolecular Junctions. *Nanotechnology* **2005**, *16*, 230.
31. Areshkin, D. A.; Gunlycke, D.; White, C. T. Ballistic Transport in Graphene Nanostrips in the Presence of Disorder: Importance of Edge Effects. *Nano Lett.* **2007**, *7*, 204–210.
32. Avriller, R.; Roche, S.; Triozon, F.; Blase, X.; Latil, S. Low-Dimensional Quantum Transport Properties of Chemically-Disordered Carbon Nanotubes: From Weak to Strong Localization Regimes. *Mod. Phys. Lett. B* **2007**, *21*, 1955–1982.
33. Cresti, A; Roche, S. Range and Correlation Effects in Edge Disordered Graphene Nanoribbons. *New J. Phys.* **2009**, *11*, 09500.